Experimental Neurology 318 (2019) 216–231

Contents lists available at ScienceDirect

Experimental Neurology

journal homepage: www.elsevier.com/locate/yexnr

Research paper

The accumulation of T cells within acellular nerve allografts is length-dependent and critical for nerve regeneration

Deng Pan[a], Daniel A. Hunter[a], Lauren Schellhardt[a], Sally Jo[a], Katherine B. Santosa[a], Ellen L. Larson[a], Anja G. Fuchs[b], Alison K. Snyder-Warwick[a], Susan E. Mackinnon[a], Matthew D. Wood[a,*]

[a] Division of Plastic Surgery, Department of Surgery, Washington University School of Medicine, St. Louis, MO 63110, USA
[b] Section of Acute and Critical Care Surgery, Department of Surgery, Washington University School of Medicine, St. Louis, MO 63110, USA

ARTICLE INFO

Keywords:
Regeneration
T cells
Peripheral nerve
Acellular nerve allograft
Schwann cells

ABSTRACT

Repair of traumatic nerve injuries can require graft material to bridge the defect. The use of alternatives to bridge the defect, such as acellular nerve allografts (ANAs), is becoming more common and desired. Although ANAs support axon regeneration across short defects (< 3 cm), axon regeneration across longer defects (> 3 cm) is limited. It is unclear why alternatives, including ANAs, are functionally limited by length. After repairing Lewis rat nerve defects using short (2 cm) or long (4 cm) ANAs, we showed that long ANAs have severely reduced axon regeneration across the grafts and contain Schwann cells with a unique phenotype. But additionally, we found that long ANAs have disrupted angiogenesis and altered leukocyte infiltration compared to short ANAs as early as 2 weeks after repair. In particular, long ANAs contained fewer T cells compared to short ANAs. These outcomes were accompanied with reduced expression of select cytokines, including IFN-γ and IL-4, within long versus short ANAs. T cells within ANAs did not express elevated levels of IL-4, but expressed elevated levels of IFN-γ. We also directly assessed the contribution of T cells to regeneration across nerve grafts using athymic rats. Interestingly, T cell deficiency had minimal impact on axon regeneration across nerve defects repaired using isografts. Conversely, T cell deficiency reduced axon regeneration across nerve defects repaired using ANAs. Our data demonstrate that T cells contribute to nerve regeneration across ANAs and suggest that reduced T cells accumulation within long ANAs could contribute to limiting axon regeneration across these long ANAs.

1. Introduction

Nerve injuries continue to be a significant public health concern, with > 300,000 patients requiring nerve surgery annually (Jaquet et al., 2001; Taylor et al., 2008). Severe traumatic injuries frequently require surgical intervention and may generate a significant tissue defect or gap between nerve ends. In these instances, a material is often necessary to bridge the nerve gap to facilitate axon growth to the distal nerve end. Autologous nerve grafts are widely considered the gold standard for surgical repair of nerve injuries resulting in a gap (Ijkema-Paassen et al., 2004). However, the use of autologous nerve grafts requires the harvest of donor nerves from patients themselves, which is undesirable. Thus, there is an unmet clinical need for "off-the-shelf" alternatives to autografts. A clinically-relevant alternative is the acellular nerve allograft (ANA), which provides an extracellular matrix (ECM) scaffold with structural elements similar to native nerve. During regeneration, cells repopulate and remodel the scaffold to promote axon regeneration. While ANAs have been increasingly used for the repair of short gap or small diameter sensory nerve injuries with results often comparable to autologous nerve grafts (Isaacs and Browne, 2014; Zhu et al., 2017), the repair of long gap or large diameter nerve injuries and motor nerve injuries with these alternatives is still tenuous, as regeneration across these alternatives can be inadequate to support recovery.

Previous animal and clinical studies have shown that repair of nerve gaps using long ANAs (> 3 cm) can result in limited axon regeneration and functional recovery (Poppler et al., 2016; Saheb-Al-Zamani et al., 2013; Xeroulis et al., 2007; Zhu et al., 2017). This length-dependent decline in regeneration across autograft alternatives is not limited to ANAs. Graft length limitations exist for collagen conduits and silicone tubes (Mokarram et al., 2017; Whitlock et al., 2009). These results suggest that there is an intrinsic limitation in regeneration across long or large, cell-free scaffolds. Specifically, our previous studies have demonstrated that failure to regenerate across long nerve gaps bridged by

* Corresponding author at: Division of Plastic and Reconstructive Surgery, Washington University in St. Louis, 660 South Euclid Avenue, St Louis, MO 63110, USA.
E-mail address: woodmd@wustl.edu (M.D. Wood).

https://doi.org/10.1016/j.expneurol.2019.05.009
Received 22 January 2019; Received in revised form 29 April 2019; Accepted 10 May 2019
Available online 11 May 2019
0014-4886/

Table 1
Experimental design.

Animal model	Treatment	Animal number	Endpoint	Analysis
Lewis (M)	2 cm ANA	6	8 weeks	Histology/histomorphometry, muscle mass
		4	4 weeks	Immunohistochemistry
		3	4 weeks	SC flow cytometry & qRT-PCR of sorted cells
		4	4 weeks	FITC-conjugated lectin perfusion analysis
		4	2 weeks	Immunohistochemistry
		4	2 weeks	qRT-PCR of cells contained within ANA
		4	2 weeks	T cell flow cytometry to quantify populations
		3	2 weeks	qRT-PCR of T cells within ANA and spleen
Lewis (F)	2 cm ANA	6	8 weeks	Histology/histomorphometry, muscle mass
Lewis (M)	2 cm ANI	6	8 weeks	Histology/histomorphometry, muscle mass
Lewis (M)	4 cm ANA	6	8 weeks	Histology/histomorphometry, muscle mass
		4	4 weeks	Immunohistochemistry
		3	4 weeks	SC flow cytometry & qRT-PCR of sorted cells
		4	4 weeks	FITC-conjugated lectin perfusion analysis
		4	2 weeks	Immunohistochemistry
		4	2 weeks	qRT-PCR of cells contained within ANA
Lewis (M)	*Re*-grafted 2 cm ANA	4	2 weeks	Immunohistochemistry
Lewis (M)	Re-grafted 4 cm ANA	4	2 weeks	Immunohistochemistry
Lewis (M)	2 cm isograft	4	8 weeks	Histology/histomorphometry
rnu/rnu (M)	2 cm isograft	4	8 weeks	Histology/histomorphometry
rnu/rnu (M)	4 cm ANA	4	8 weeks	Histology/histomorphometry
rnu/rnu (M)	2 cm ANA	8	8 weeks	Histology/histomorphometry, muscle mass, SFI
rnu/+ (M)	2 cm ANA	8 (7)	8 weeks	Histology/histomorphometry, muscle mass, SFI

acellular alternatives (like ANAs) is due to how cells repopulate ANAs rather than the intrinsic failure of motor and sensory neurons to regenerate their axons across long distances (Poppler et al., 2016).

While our previous studies suggest that altered Schwann cell functions or phenotypes could be causal to limited axon regeneration across long ANAs, there are a variety of cells that repopulate ANAs in addition to Schwann cells. Leukocytes, such as macrophages, are some of the first cells to respond to tissue injury and play a critical role in facilitating tissue regeneration upon acellular scaffolds. Therefore, in turn, the disruption of leukocyte repopulation or functions can impact regeneration. Specifically, the dysfunction of macrophages or T cells has been implicated in poor regeneration of skin, heart, and central nervous system tissues (Hesketh et al., 2017; Lavine et al., 2014; Loots et al., 1998; Sindrilaru et al., 2011).

Macrophages are required for proper angiogenesis following injury. The depletion of macrophages in the context of peripheral nerve injury can lead to deficient angiogenesis and poor Schwann cell migration (Cattin et al., 2015). Additionally, recent studies demonstrate that macrophages play a role in modulating Schwann cell functions (Stratton et al., 2018). Other studies have found that nerve repaired with a conduit containing a greater proportion of macrophages with CD206 expression is associated with better regenerative outcomes, suggesting macrophage phenotype can impact nerve regeneration through cell-free scaffolds (Mokarram et al., 2017, 2012). While these data suggest that macrophages play important roles in nerve regeneration, limited data are available regarding how macrophage functions might differ based on scaffold length.

Similar to macrophages, T cells are critical for regeneration in many organ systems (Burzyn et al., 2013; Epelman et al., 2015; Walsh et al., 2015; Zhang et al., 2014). In general, T cells can modulate regeneration through a variety of mechanisms including secretion of cytokines, release of growth factors, or direct cell-cell interaction (Burzyn et al., 2013; Ishii et al., 2012; Pull et al., 2005). But, the role of T cells in peripheral nerve regeneration is far from resolved. Additionally, the majority of studies on T cells' roles in nerve have not yet considered the role of T cells during nerve regeneration across a scaffold, such as during nerve defect repair. In this scenario, there is a high demand for cell migration and repopulation, including extensive angiogenesis, to bridge the scaffold and facilitate axon regeneration. As an example of T cells' role in this context, T cells were critical to robust muscle regeneration when acellular scaffolds were used to repair muscle defects (Sadtler et al., 2016). Therefore, T cells may play a more prominent role in nerve regeneration across acellular scaffolds, such as ANAs.

In this study, we focused on determining regenerative differences between ANAs based on their length. We specifically focused on leukocytes (i.e. macrophages and T cells) repopulating these ANAs, where we uncovered novel differences in adaptive immunity responses between ANAs based on length. Furthermore, from these findings we confirmed a role for T cells in mediating regeneration across ANAs.

2. Materials and methods

2.1. Reagents and chemicals

All reagents, consumables, and chemicals, unless otherwise stated, were purchased from Sigma-Aldrich (St. Louis, MO).

2.2. Animals and experimental design

Commercially-available adult rats (200-250 g, Charles River Laboratories, Wilmington, MA) were utilized for all experiments. Sprague-Dawley rats were used as donor nerve for processing to generate ANAs. Lewis rats were used to generate isografts or acellular nerve isografts (ANIs). For most experimental groups, Lewis rats were used, as these are a well-accepted rat strain to study nerve regeneration. To assess the effects of T cells on regeneration across ANAs, athymic rats were used in experimental groups. Both T cell deficient homozygote (rnu/rnu) and T cell-sufficient heterozygote (rnu/+) athymic rats were included in order to allow for direct comparison between rats derived from a matching genetic background. This comparison minimizes confounding factors associated with any potential differences in nerve recovery between rat strains. Surgical procedures and peri-operative care measures were conducted in compliance with the AAALAC accredited Washington University Institutional Animal Care and Use Committee (IACUC) and the National Institutes of Health guidelines. All animals were housed in a central animal care facility and provided with food (PicoLab rodent diet 20, Purina Mills Nutrition International, St. Louis, MO) and water ad libitum.

The studies included multiple independent sets of animals in order to measure a variety of different outcome metrics (Table 1). For groups, rat sciatic nerve was transected and repaired using either an ANA or isograft as indicated in Table 1. Studies in Lewis rats assessed how ANA

length affected nerve regeneration across the ANA. The extent of nerve regeneration was measured at 8 weeks post operatively using histology and histomorphometry. To assess early regenerative processes, both 2 and 4 weeks were chosen as endpoints to capture cell repopulation and changes to gene expression contained within ANAs. Finally, the role of ANA length on early regenerative outcomes was assessed using a "re-grafting" experiment (see "Surgical Procedures"). After comparing ANAs based on length and identifying a potential role for T cells during nerve regeneration, the role of T cells in nerve regeneration was assessed. By considering nerve repaired using 2 cm ANAs in Lewis rats, as ANAs at this length successfully promoted regeneration and yielded robust accumulation of T cells sufficient for quantification, T cells were additional characterized at 2 weeks using cell sorting and gene analysis. To determine if the foreign nature of the ANA contributed to nerve regeneration, Lewis rat nerve was repaired using either ANAs or ANIs and evaluated for the extent of nerve regeneration at 8 weeks employing the same outcome metrics used previously. Finally, to assess the T cell role directly, athymic rats had their nerves repaired using either isografts or ANAs. The extent of nerve regeneration across these grafts was assessed at 8 weeks using histology and histomorphometry, relative muscle mass, and sciatic functional index. During surgery on athymic rats, a single rnu/+ rat died unexpectedly.

The group size for each metric was selected based on prior studies and power analysis. For assessing the extent of nerve regeneration at 8 weeks, we determined the minimum sample size for $\alpha = 0.05$, with a two-tailed *t*-test and at a statistical power level of 80%. It was estimated from the literature and our previous experience with rodent animal models that a standard deviation of ~20% of the mean is reasonable for the nerve regeneration outcomes proposed. Therefore, $n = 6$ per group in rodent sets would allow for adequate detection ($\beta = 0.80$) of differences in means between two groups for an effect size of at least 50%, while $n = 8$ per group at similar conditions would allow for detection of an effect of at least 30%. For analysis of immunohistochemistry, gene expression, and cell sorting, we expected to see greater effect sizes and less variance, and thus the numbers per group in these sets was less.

2.3. Surgical procedures

For procedures, rats were anesthesized using a cocktail of ketamine (75 mg/kg; Fort Dodge Animal Health, Fort Dodge, IA) and dexmedetomidine (0.5 mg/kg; Pfizer Animal Health, Exton, PA). For rats serving as graft donors, following euthanization, the sciatic nerve was exposed at the level of the trifurcation, and the dissection was extended proximally to the level of exiting nerve roots at the cruciate ligaments yielding ~4.5-5 cm of nerve. From the harvested nerve, it was trimmed to the appropriate length for isograft or first processed (see below) and then trimmed to the appropriate length (20 mm or 40 mm lengths as necessary). In experimental rats, the right sciatic nerve was exposed and transected 5 mm proximal to the distal trifurcation. The indicated grafts were reversed (distal end of donor graft facing proximal nerve stump of recipient) sutured into the nerve gap with 9–0 nylon microsuture (Sharpoint, Reading, PA). The grafted nerves were shaped like a loop and inserted into an under-skin "pocket" around the femur as previously described for placement of long nerve grafts (Hoben et al., 2018; Poppler et al., 2016; Saheb-Al-Zamani et al., 2013; Yan et al., 2018). The sigmoidal nature of this path does not significantly interfere with regeneration (Kawamura et al., 2005).

For re-grafting experiments, a set of animals was first repaired using 2 cm or 4 cm ANAs as just described. Then, under anesthesia, these ANAs were harvested and trimmed to equal lengths (1.5 cm) at the mid-graft region at 2 weeks post-repair. These 1.5 cm pre-grafted ANAs were then used to repair freshly transected nerves ("re-grafted") in new rats using similar procedures as just described.

For all rats following nerve repair, a two-layer closure of muscle and skin was performed using 6–0 vicryl and 4–0 nylon suture, respectively. Atipamezole solution (0.1 mg/kg; Zoetis, Florham Park, NJ) was administered for anesthesia reversal. The animals were recovered on a warming pad and monitored for postoperative complications before returning them to a central animal care facility. Postoperative pain was managed using Buprenorphine SR™ (0.05 mg/kg; ZooPharm, Windsor, CO). Animals were monitored daily post-operatively for signs of infection and/or distress. At the appropriate endpoints, animals were euthanized with injection of Somnasol (150 mg/kg; Delmarva Laboratories) and their nerves collected for respective studies (see below).

2.4. ANA processing

ANAs were decellularized using a modified series of detergents in the method described previously (Poppler et al., 2016). Nerves isolated from donor animals the nerves were repeatedly washed in deionized water and three detergents in a sodium phosphate buffer: Triton X-100, sulfobetaine-16 (SB-16), and sulfobetaine-10 (SB-10). All grafts were washed and stored in 10 mM phosphate-buffered 50 mM sodium solution at 4 °C and used within 3 days.

2.5. Histology and histomorphometry

To quantify the extent of nerve regeneration, histology and histomorphometric analysis of nerve were performed as previously described (Hunter et al., 2007). Briefly, tissue was collected and fixed via immersion in 3% glutaraldehyde (Polysciences, Inc., Warrington, PA), then post-fixed in 1% osmium tetroxide, and serially dehydrated. These tissues were embedded in epoxy resin (Polysciences) and sectioned on an ultramicrotome for 1.5 μm cross sections. Slides were then counterstained with 1% toluidine blue dye and analyzed at 1000× overall magnification on a Leitz Laborlux S microscope. A semi-automated digital image-analysis system linked to morphometry macros developed for peripheral nerve analysis (Clemex Vision Professional, Clemex Technologies, Longueuil, Québec), was used. Six random fields per histological section were imaged by a person blinded to the experiments resulting in ~75% of the available nerve cross-sectional area imaged. Binary histomorphometry analysis of the digitized information based on gray and white scales allowed measurements of total fascicular area and total fiber number in the relevant nerve sections. Further counting of myelinated fibers across multiple randomly selected fields per nerve permitted calculation of nerve fiber density (fibers/mm2), total number of myelinated fibers, distribution of myelinated fiber width (μm2), percent myelinated fiber and percent fiber debris. These numbers were averaged across the six images to obtain counts for a single animal ($n = 1$).

2.6. Relative muscle mass

To further quantify the extent of nerve regeneration, relative gastrocnemius muscle mass was measured as it is indicative of reinnervation of denervated muscles. After nerve harvest, the gastrocnemius muscles were harvested from the experimental and contralateral sides of rats. Wet muscle weight was recorded on each side, and the ratio of the ipsilateral to contralateral muscle weight was calculated.

2.7. Sciatic function index

To further quantify the extent of nerve regeneration, starting from 6 weeks after surgery, athymic rats underwent walking track assessment to determine functional recovery. Lewis rats developed contractures in the affected foot that prevented meaningful assessment in recovery. Rat hind feet were glazed with non-toxic paint to track at least 3 pairs of footprints. Using these footprints, the sciatic functional index (SFI) was calculated.

2.8. Immunohistochemistry

To assess cell composition and populations within ANAs, nerve samples were explanted at the endpoints described and immediately placed in 4% paraformaldehyde in phosphate-buffer overnight followed by immersion in 30% sucrose in PBS solution for 24–48 h. Samples were then frozen in OCT Compound (VWR, Radnor, PA) and sectioned at 15 μm onto pretreated charged glass slides. Sections were rehydrated with PBS and blocked using 5% normal goat serum diluted in PBS before primary antibody staining. Primary antibodies were used to stain for Schwann cells (S100), cell proliferation (Ki-67), endothelial cells (RECA-1), macrophages (CD68, CD206), and T cells (CD3, CD4). Primary antibody in 5% serum buffer was applied and incubated at 4 °C overnight with antibodies and concentrations outlined in Supplementary Table 1. Sections were then washed in PBS and stained for the appropriate fluorochrome-conjugated secondary antibodies for 1 h at room temperature. All sections were mounted with Fluoroshield mounting medium with DAPI (Abcam, Boston, MA) and then imaged using the Fluoview FV1000 confocal microscope and acquisition system (Olympus, Waltham, MA) at overall 200× (20× water immersion objective) or 600× magnification (60× oil immersion objective). A minimum of three sections were analyzed and averaged for each tissue area using ImageJ (NIH) to obtain a value for each single animal ($n = 1$). For percent area, an ImageJ macro was used to quantify the percentage of the area in a standardized field that was positive for the marker measured. For cell counts, field size was kept standard at a 60× objective (600× magnification overall), and colocalization of the primary marker(s) with DAPI was considered a positive cell.

2.9. FITC-conjugated lectin perfusion analysis

To visualize functional blood vessels, 500 μg of FITC conjugated lectin (Vector Lab, Burlingame, CA) was injected intravenously into each animal under anesthesia. Five minutes after injection, the ANA graft was explanted, and the animal sacrificed. Grafts were fixed and sectioned similar to the details described in the "Immunohistochemistry" section. Functional vessels were visualized by its fluorescence due to binding of FITC-lectin and quantified as percent area, similar to methods as just described for immunohistochemistry.

2.10. Cell sorting

To further characterize Schwann cells and T cells within ANAs during ongoing regeneration, these cells were isolated from ANAs. ANAs were explanted from rats at described endpoints after nerve repair and finely minced. Each sample/animal ($n = 1$) was then incubated with 1 mL of digestion buffer (0.1% collagenase, 0.05% DNase in 2% fetal bovine serum (FBS)/ Dulbecco's Modified Eagle Media (DMEM)). Samples were incubated for 20 min at 37 °C with constant agitation. Following digestion, the samples were re-suspended in FACS buffer (2% FBS, 0.1% EDTA in phosphate buffered saline) and filtered through a 70 μm sized cell strainer. Cells were then incubated with anti-CD32 for 10 min and then incubated with a cocktail of CD45-PE-Cy7, Thy1-PerCP, and O4-PE for sorting of Schwann cells. (Irigoyen et al., 2018; Lutz, 2014). For staining of T cells, cells were incubated with a cocktail of CD45-PE, CD11bPE/Cy7, CD3 PerCP, CD4 FITC, CD8 Pacific blue. Cells were then washed and resuspended in FACS buffer. Cells were sorted on Aria II (BD Bioscience, San Jose, CA) at the Washington University Flow Cytometry core. Schwann cells were sorted by $CD45^-Thy1^-O4^+$. T cells were sorted by $CD45^+CD11b^-CD3^+$.

2.11. RT-PCR

To quantify gene expression from all cells within ANAs or from individual sorted cell populations (SCs and T cells) obtained from ANAs (see "Cell sorting" section), qRT-PCR was performed focused on select panels of genes (Supplemental Table II). For SCs, these genes included myelination and maturation genes (Ghislain and Charnay, 2006), as well as activation or "repair" phenotype genes (Arthur-Farraj et al., 2012). For ANAs and T cells, genes were focused on a panel of inflammatory cytokines related to T cell functions. Total RNA was prepared from either flow sorted cells or ANA explants. RNA was extracted using Trizol (Life Technologies), chloroform and an RNeasy Kit (Qiagen, Valencia, CA) according to manufacturer's instructions. RNA concentration was determined on a NanoDrop 1000 Spectrophotometer (Thermo Scientific, Wilmington, DE). The cDNA was generated with SuperScript II reverse transcriptase (Invitrogen, Carlsbad, CA). Real-time PCR was performed using a Step One Plus thermocycler (Applied Biosystems, Foster City, CA) using Taqman Master Mix (Applied Biosystems) reagents with specific oligonucleotide primer pairs (Supplemental Table II). The PCR conditions were 50 °C for 2 min and then 95 °C for 15 s and 60 °C for 1 min, repeated for 40 cycles, with a hot start at 95 °C for 10 min. The expression levels of each gene were normalized to those of the internal control gene (*Actb*). Data was analyzed using Step One Software v2.2.2 (Applied Biosystems, Foster City, CA).

2.12. Cell culture (Supplemental Data)

To determine if the T cell-related cytokine IFN-γ could affect Schwann cells, rat Schwann cells were isolated from uninjured, adult Lewis rat sciatic nerves. Isolated nerves were de-sheathed and digested with digestion cocktail of 0.1% collagenase in DMEM and 2% FBS. Isolated cells were then cultured on PLL-laminin coated plates until confluence in DMEM, 10% FBS with 2 μM forskolin. To purify the Schwann cells, cells were treated with rabbit anti-thy1 IgM at room temperature followed by complement mediated lysis using rabbit complement. Schwann cells purity was determined by staining with S100. When indicated, Schwann cells were plated onto PLL coated cell culture dish with serum free medium (DMEM, 0.1% BSA, 1× N2 supplement) with or without 10 nM IFN-γ (Peprotec, Rock Hill, NJ).

2.13. Statistical analysis

Statistical analyses were performed using GraphPad Prism. Each animal and its nerve was considered an 'n' value. All data were compiled as mean ± standard deviation. Data were tested for normality using the Kolmogorov–Smirnov test. Student's *t*-test was performed for comparisons between 2 groups. A significance level of $p < 0.05$ was used in all statistical tests performed.

3. Results

3.1. Regenerative capacity of ANAs depends on ANA length

In male Lewis rats, the repair of nerve gaps using 2 cm or 4 cm ANAs revealed nerve regeneration across the ANA was length-dependent. At an 8 week endpoint as shown in Fig. 1A, we found robust myelinated axon regeneration to the mid-graft when nerves were repaired using 2 cm ANAs, where nearly 10,000 myelinated axons were found to have regenerated. Conversely, regeneration across 4 cm ANAs was inferior, where the mid-graft of nerve repaired with 4 cm ANAs contained < 1000 myelinated axons ($p < 0.0001$). Furthermore, as we examined the distal nerves for axonal regeneration (Fig. 1B), we found that while nerve repaired with 2 cm ANAs maintained almost 10,000 myelinated axons, there were almost no observable myelinated axons in the distal stump when repaired with 4 cm ANAs ($p < 0.0001$). Relative gastrocnemius muscle mass was significantly greater for nerve repaired using 2 cm compared to 4 cm ANA ($p < 0.0001$; Fig. 1C). We also compared regenerative outcomes among male and female rats receiving nerve repair using 2 cm ANAs finding similar outcomes in females indicating no sex differences (Fig. S1). These results demonstrate that ANAs can support robust axon regeneration up to a certain length.

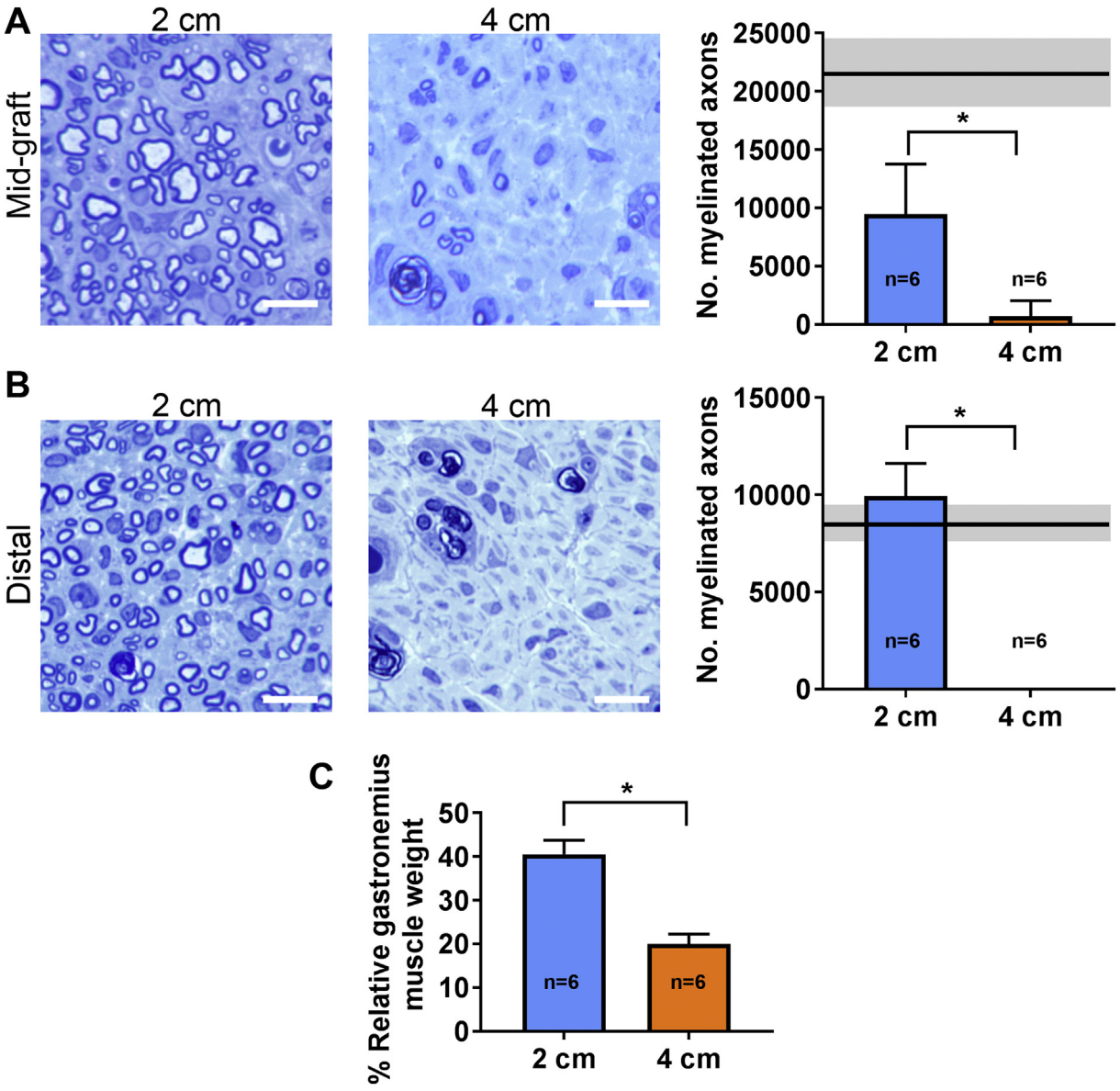

Fig. 1. ANAs facilitate axon regeneration in a length dependent manner. Eight weeks after nerve repair using either 2 cm or 4 cm ANAs, the extent of axon regeneration to the A) mid-graft of ANA and B) distal nerve was quantified. At this same endpoint, C) relative gastrocnemius muscle weight was also measured. Representative histological images of nerve are shown, where white scale bar is 20 μm. Data represented as mean ± SD; $p < 0.001$ for both mid-graft and distal nerve; Solid line with gray area represents number of myelinated axons when nerves are repaired with 2 cm isografts. $p < 0.05$ for muscle weights.

3.2. Schwann cells repopulating ANAs differ based on ANA length

The profoundly reduced axon regeneration across long ANAs suggests disrupted earlier regenerative processes that would normally promote axon growth, such as SC ($S100^+$) repopulation of ANAs. Evaluating these ANAs at a 4 week endpoint, the mid-graft of 2 cm ANAs contained approximately 3-fold greater $S100^+$ area compared to 4 cm ANAs ($p = 0.0195$; Fig. 2A-B). Furthermore, we found that nearly 10% of $S100^+$ cells in the mid-graft of 2 cm ANAs expressed Ki-67, while < 2% of $S100^+$ cells in the 4 cm ANAs expressed Ki-67 ($p = 0.0067$; Fig. 2C).

To further understand the phenotype of SCs, we isolated SCs from within these ANAs and characterized their gene expression. Overall, there were no significant differences in the number of SCs isolated per cm (density) from either 2 cm or 4 cm ANAs (Fig. 2D-E). Despite the similar density of SCs, the gene expression of SCs from 2 cm ANAs differed from those within 4 cm ANAs. We found the SCs contained within 2 cm vs 4 cm ANAs expressed greater levels of genes related to maturation and myelination ($p < 0.05$; Fig. 2F), including *Krox20*, *Mbp*, *Mpz*, and *Pmp2*. Select genes related to activation, including *C-Jun* and *Mmp9*, were expressed to a greater extent in SCs from 2 cm ANAs ($p < 0.05$; Fig. 2G). Taken together, these data demonstrate SC accumulation and functions differ based on ANA length and suggest that SCs in 2 cm ANAs are more functional, while SCs in 4 cm ANAs resemble quiescent or senescent-like cells.

3.3. Angiogenesis is affected by ANA length

As robust and precise angiogenesis contributes to SC functions (Cattin et al., 2015; Cattin and Lloyd, 2016), we assessed if angiogenesis differed among ANAs based on ANA length. Four weeks after nerve repair, while both 2 and 4 cm ANAs contained functional vessels, the mid-graft of 2 cm ANAs had 2-fold greater $FITC^+$ Lectin area compared to 4 cm ANAs ($p = 0.0315$; Fig. 3A). Furthermore, at both 2 weeks ($p = 0.0153$), and 4 weeks ($p = 0.0126$) post-repair, the mid-graft of 2 cm ANAs had approximately 2-fold greater RECA-1^+ area compared

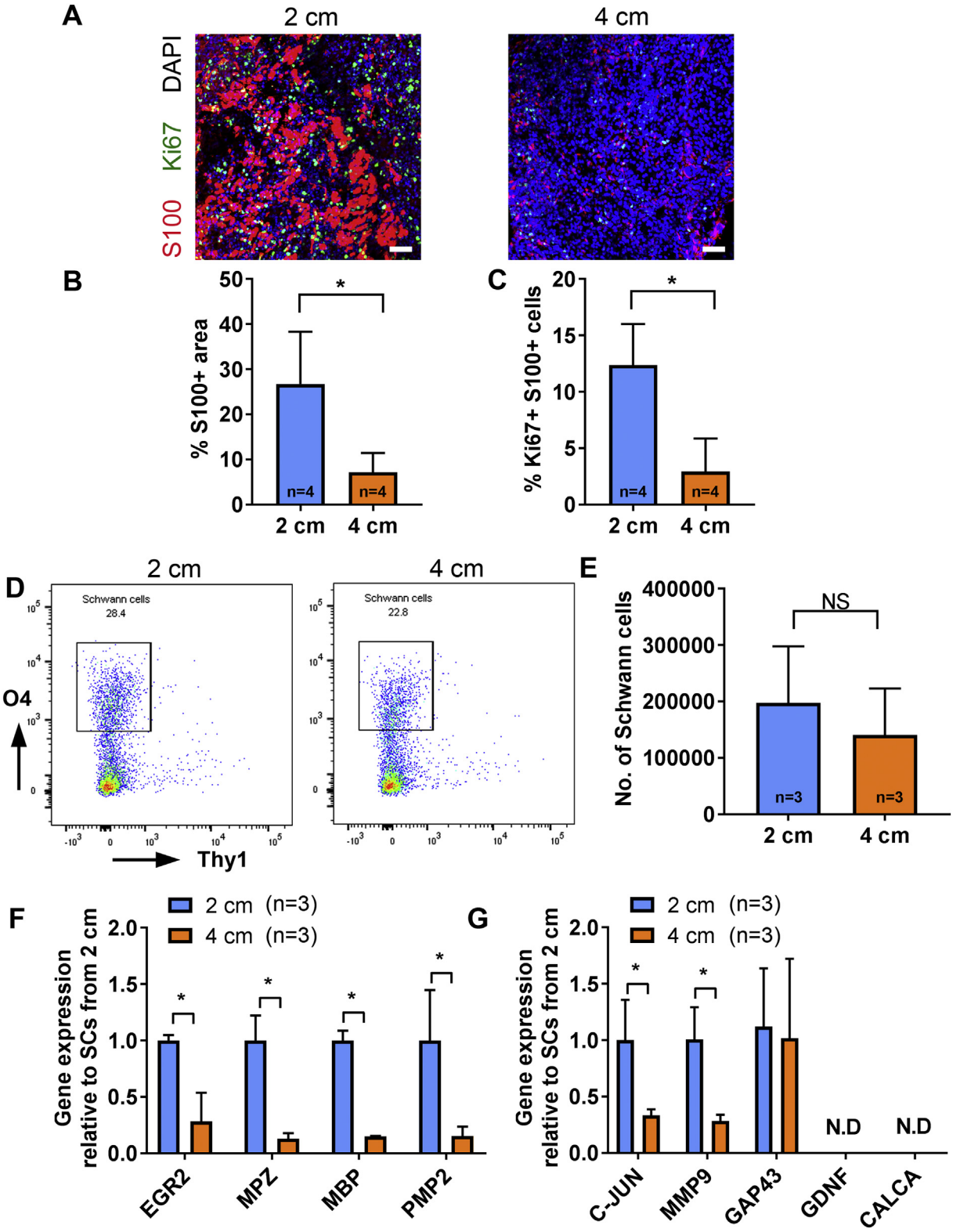

Fig. 2. Schwann cell phenotypes differ in nerves repaired with short (2 cm) or long (4 cm) ANAs. Four weeks after nerve repair using ANAs, SC quantity and phenotype within mid-graft of 2 cm and 4 cm ANAs were assessed. A) Representative IHC for S100 (red) and Ki-67 (green). Scale bar represent 20 μm. B) Quantification of S100+ area and C) proportion of Ki-67+ Schwann cells. Data represented as mean ± SD; * indicates $p < 0.01$. Similarly, SCs were isolated from the entirety of these ANA using FACS. D) Representative flow cytometry showing gating of CD45-Thy1-O4+ Schwann cells, and E) quantification of Schwann cells per cm of graft from either 2 cm or 4 cm grafts. SCs sorted from FACS were used to probe for gene expression using real time RT-PCR. Quantification of SC F) activation related and G) maturation related gene expression. Data represented as mean ± SD; * indicates $p < 0.01$; ns: not significant. (For interpretation of the references to colour in this figure legend, the reader is referred to the web version of this article.)

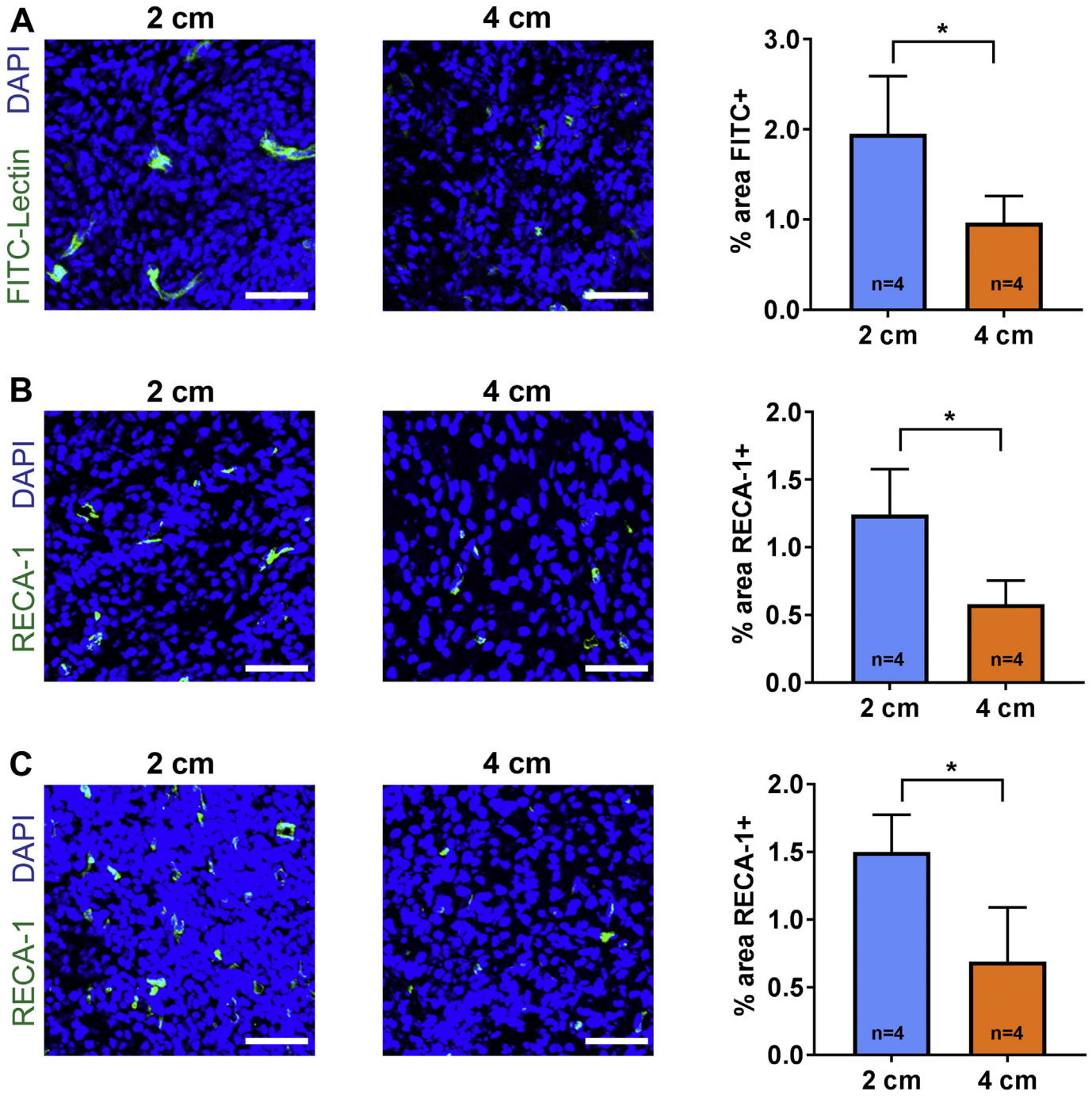

Fig. 3. Angiogenesis differs among short (2 cm) or long (4 cm) ANAs. After nerve repair using ANAs, angiogenesis within mid-graft of 2 cm and 4 cm ANAs was assessed. A) Representative IHC images of perfused FITC-conjugated lectin (green) with quantification 4 weeks after ANA repair. At B) 4 weeks and C) 2 weeks, angiogenesis was assessed using IHC RECA-1 (green) to identify endothelial cells. Representative IHC images of mid-graft for 2 cm or 4 cm ANA with quantification of RECA-1 + area. Data represented as mean ± SD; * indicates $p < 0.05$. Scale bars represent 40 μm. (For interpretation of the references to colour in this figure legend, the reader is referred to the web version of this article.)

to 4 cm ANAs, suggesting a greater quantity of endothelial cells in 2 vs 4 cm ANAs (Fig. 3B-C). Overall, these data demonstrate long ANAs have disrupted angiogenesis, as compared to shorter ANAs.

3.4. Leukocyte response is affected by ANA length

As macrophages mediate angiogenesis following nerve injury, we compared macrophage quantities and phenotype within 2 vs 4 cm ANAs. We found that 2 weeks after repair, macrophages ($CD68^+$) began to accumulate within ANAs. $CD68^+$ cells represented about 35–40% of total cells in ANAs. However, despite differences in SCs and angiogenesis, there were no differences in $CD68^+$ cell quantities among 2 vs 4 cm ANAs at 2 weeks, nor differences in the proportion of $CD206^+CD68^+$ cells ($CD206^+$ or M2 macrophages) (Fig. 4A-C). At 4 weeks, $CD68^+$ cell quantities contained in either length ANA at the mid-graft were substantially reduced compared to 2 weeks. However, the relative proportion of $CD206^+CD68^+$ cells of total $CD68^+$ cells increased in ANAs of either length. Then, comparing 2 and 4 cm ANAs to one another at 4 weeks, the total number of $CD68^+$ cells in 2 cm ANAs were almost double compared to 4 cm ANAs (8% vs 5% of total

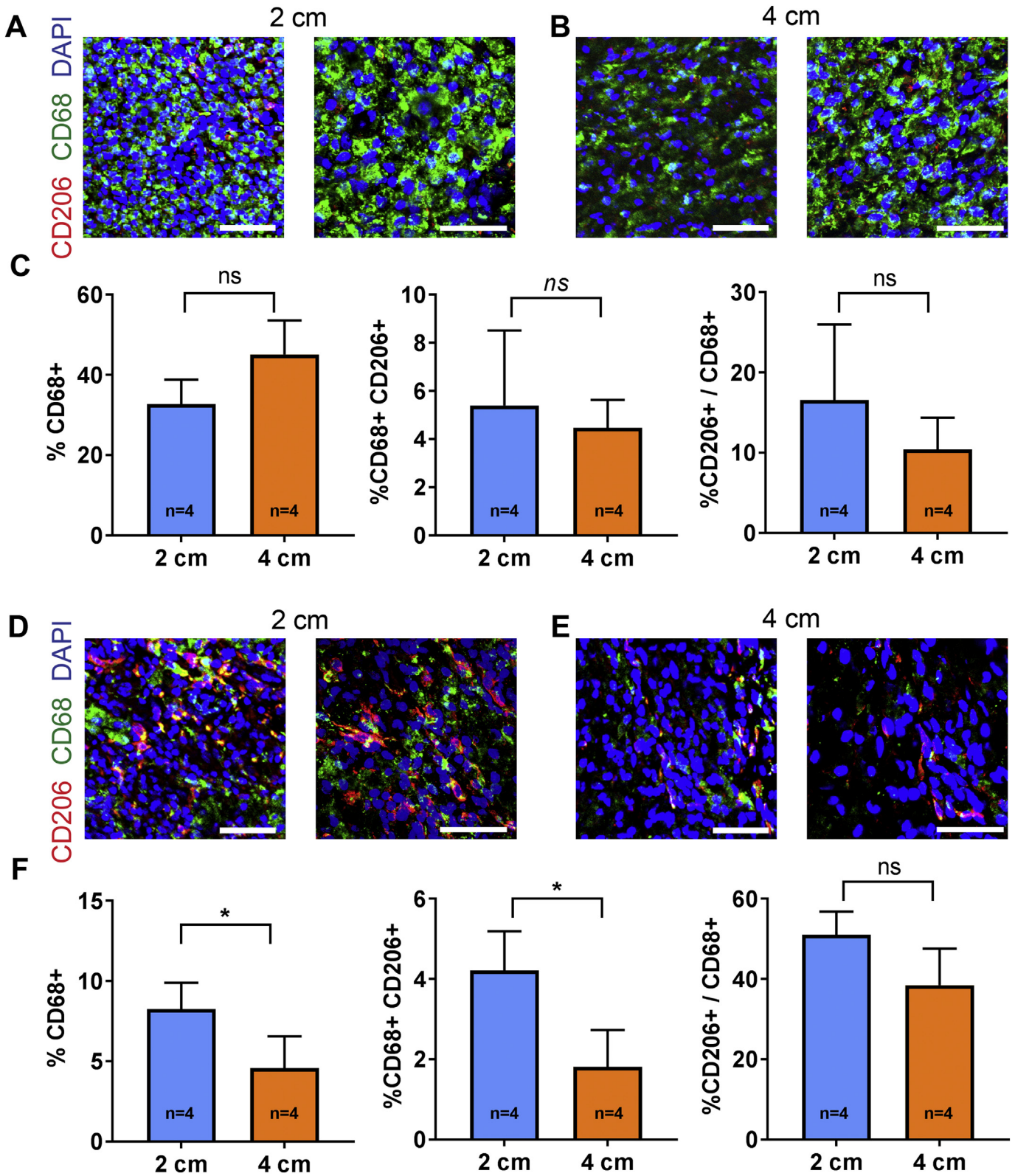

Fig. 4. Macrophage accumulation has minimal changes among short (2 cm) or long (4 cm) ANAs. After nerve repair using ANAs, macrophage accumulation within mid-graft of 2 cm and 4 cm ANAs was assessed A-C) 2 weeks and D-F) 4 weeks following repair. Two weeks after repair, representative IHC images of CD206 (red) and CD68 (green) from mid-graft of A) 2 cm ANAs, and B) 4 cm ANAs. C) The proportion of CD68+ cells, CD206+ CD68+ cells, and proportion of CD206+ cells among CD68+ cells was quantified. Four weeks after repair, representative IHC images of CD206 (red) and CD68 (green) from mid-graft of D) 2 cm ANAs, and E) 4 cm ANAs. F) The proportion of CD68+ cells, CD206+ CD68+ cells, and proportion of CD206+ cells among CD68+ cells was quantified. Data represented as mean ± SD; * indicates $p < 0.05$; ns: not significant. (For interpretation of the references to colour in this figure legend, the reader is referred to the web version of this article.)

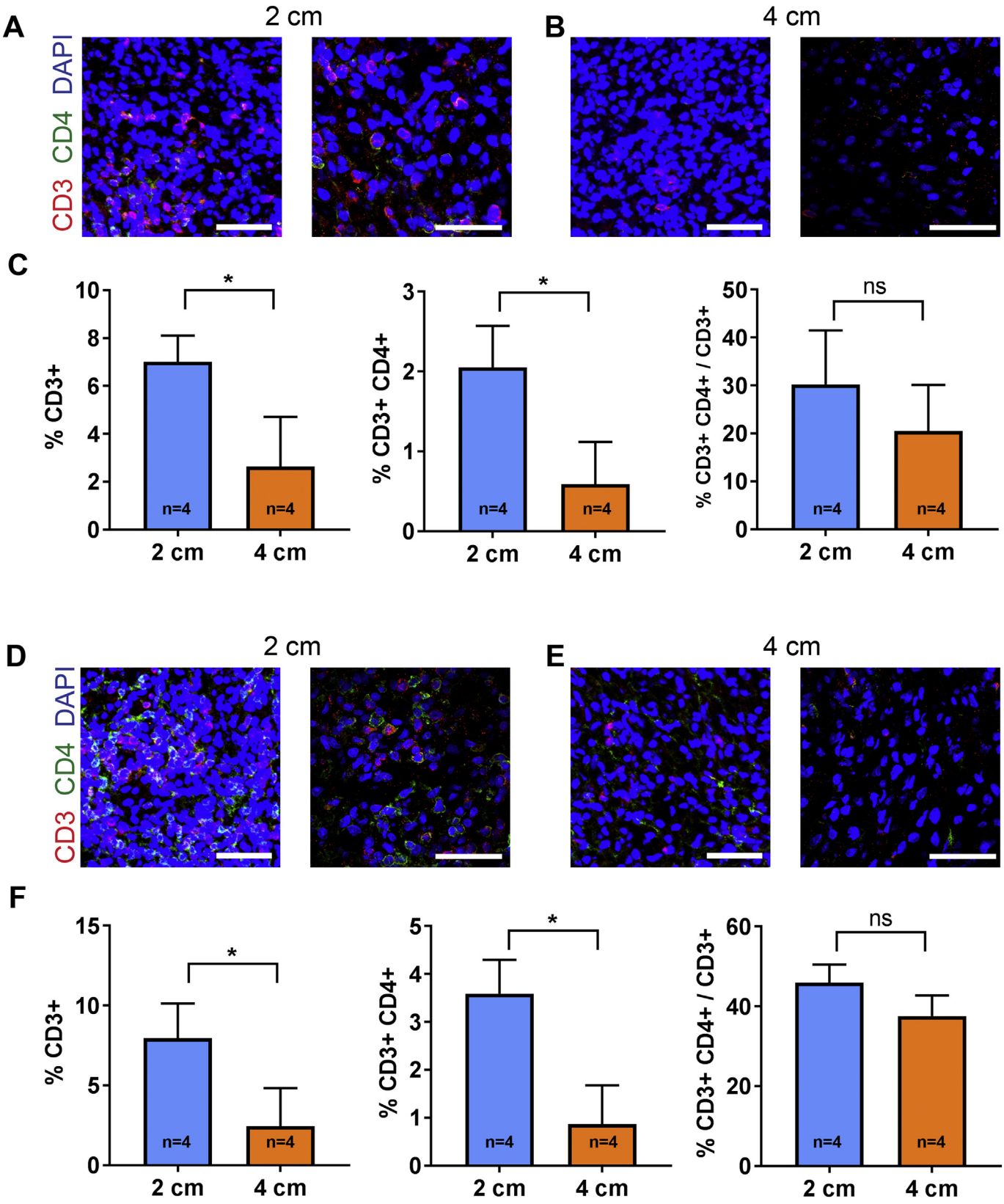

Fig. 5. T cell accumulation is reduced in long (4 cm) ANAs. After nerve repair using ANAs, T cell accumulation within mid-graft of 2 cm and 4 cm ANAs was assessed A-C) 2 weeks and D-F) 4 weeks following repair. Two weeks after repair, representative IHC images of CD206 (red) and CD68 (green) from mid-graft of A) 2 cm ANAs, and B) 4 cm ANAs. C) The proportion of CD3+ cells, CD3+ CD4+ cells, and proportion of CD4+ cells among CD3+ cells was quantified. Four weeks after repair, representative IHC images of CD206 (red) and CD68 (green) from mid-graft of D) 2 cm ANAs, and E) 4 cm ANAs. F) The proportion of CD3+ cells, CD3+ CD4+ cells, and proportion of CD4+ cells among CD3+ cells was quantified. Data represented as mean ± SD; * indicates $p < 0.05$; ns: not significant. (For interpretation of the references to colour in this figure legend, the reader is referred to the web version of this article.)

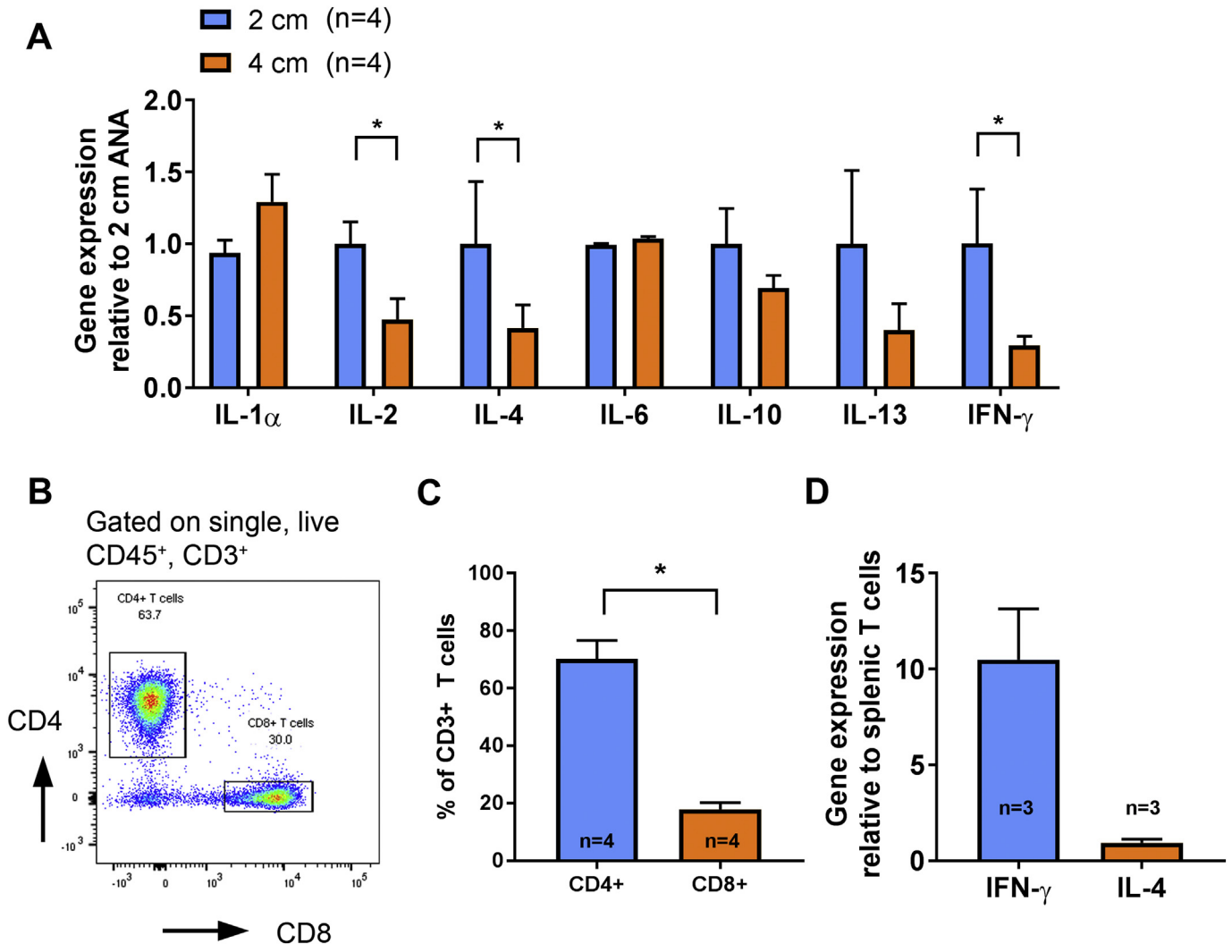

Fig. 6. Cytokine expression differs based upon ANA length. A) Two weeks after nerve repair using ANA, gene expression from cells contained within 2 cm and 4 cm ANAs was measured using RT-PCR. * indicates $p < 0.05$. Additionally, T cells were isolated from the entirety 2 cm ANA using FACS. B) Representative flow cytometry of 2 cm ANAs gated CD45 + CD11b-CD3+ cells. C) Quantification of the proportion of CD4+ and CD8+ cells among CD3+ cells. D) Quantification of IFN-γ and IL-4 gene expression from T cells isolated from 2 cm ANAs. All data represented as mean ± SD; * indicates $p < 0.01$.

cells for 2 cm and 4 cm, respectively; $p = .0289$; Fig. 4D-F). In turn, 4 cm ANAs also accumulated fewer total $CD206^+CD68^+$ cells compared to 2 cm ANAs. However, the relative proportion of $CD206^+CD68^+$ cells were not different between 2 cm and 4 cm ANAs. Overall, these data demonstrate that macrophage accumulation within ANAs based on length does not differ until 4 weeks.

As T cells can be an integral to cell functions, including macrophages, during regeneration (Burzyn et al., 2013; Nishimura et al., 2009; Zhang et al., 2014; Sadtler et al., 2016), we also assessed T cell accumulation within ANAs. The infiltration of T cells ($CD3^+$) into ANAs was observed as early as 2 weeks following repair (Fig. 5A-B). At 2 weeks, the total number of $CD3^+$ cells in the mid-graft of 2 cm ANAs (~7% of total cell numbers) was nearly 3-fold greater than that of 4 cm ANAs ($p = 0.0096$; Fig. 5C). While the total number of $CD3^+$ cells greatly differed between 2 vs 4 cm ANAs, both 2 cm and 4 cm ANAs contained nearly identical proportions of double positive $CD4^+$ $CD3^+$ cells, representing almost 30% of all $CD3^+$ cells. At 4 weeks, the total proportion of $CD3^+$ cells in 2 cm ANAs remained consistent to the values at 2 weeks (~7–8% of total cells; Fig. 5D-F). However, $CD3^+$ cells represented only about 2% of total cells in 4 cm ANAs ($p = 0.0142$). Again at 4 weeks, both 2 cm and 4 cm ANAs contained nearly identical proportions of $CD4^+$ $CD3^+$ cells, now representing approximately 40% of all $CD3^+$ cells. Overall, these data demonstrate that T cells accumulate to a greater extent within short ANAs.

3.5. Cytokine expression is altered based on ANA length

To further assess inflammation, inflammatory gene expression from cells contained within ANAs and from T cells was assessed. Comparing gene expression from cells contained within ANAs, 2 cm ANAs contained upregulated expression of a variety of pro- and anti-inflammatory cytokines including IL-2, IL-4, and IFN-γ compared to 4 cm ANAs ($p = 0.0024$, $p = 0.0446$, and $p = 0.01$, respectively; Fig. 6A). T cells from 2 cm ANAs were further characterized. $CD4^+$ $CD3^+$ cells represented a five-fold greater majority of $CD3^+$ cells within 2 cm ANAs compared to $CD8^+$ $CD3^+$ cells ($p = 0.0002$; Fig. 6B-C). $CD3^+$ cells within 2 cm ANAs showed no change in the RNA level of IL-4, but IFN-γ was upregulated compared to splenic $CD3^+$ cells (Fig. 6D). Therefore, altered cytokine expression contained within ANAs could be partly due to T cells.

3.6. ANA length limits angiogenesis and T cell accumulation within ANAs

As the extent of angiogenesis and T cell accumulation are reduced

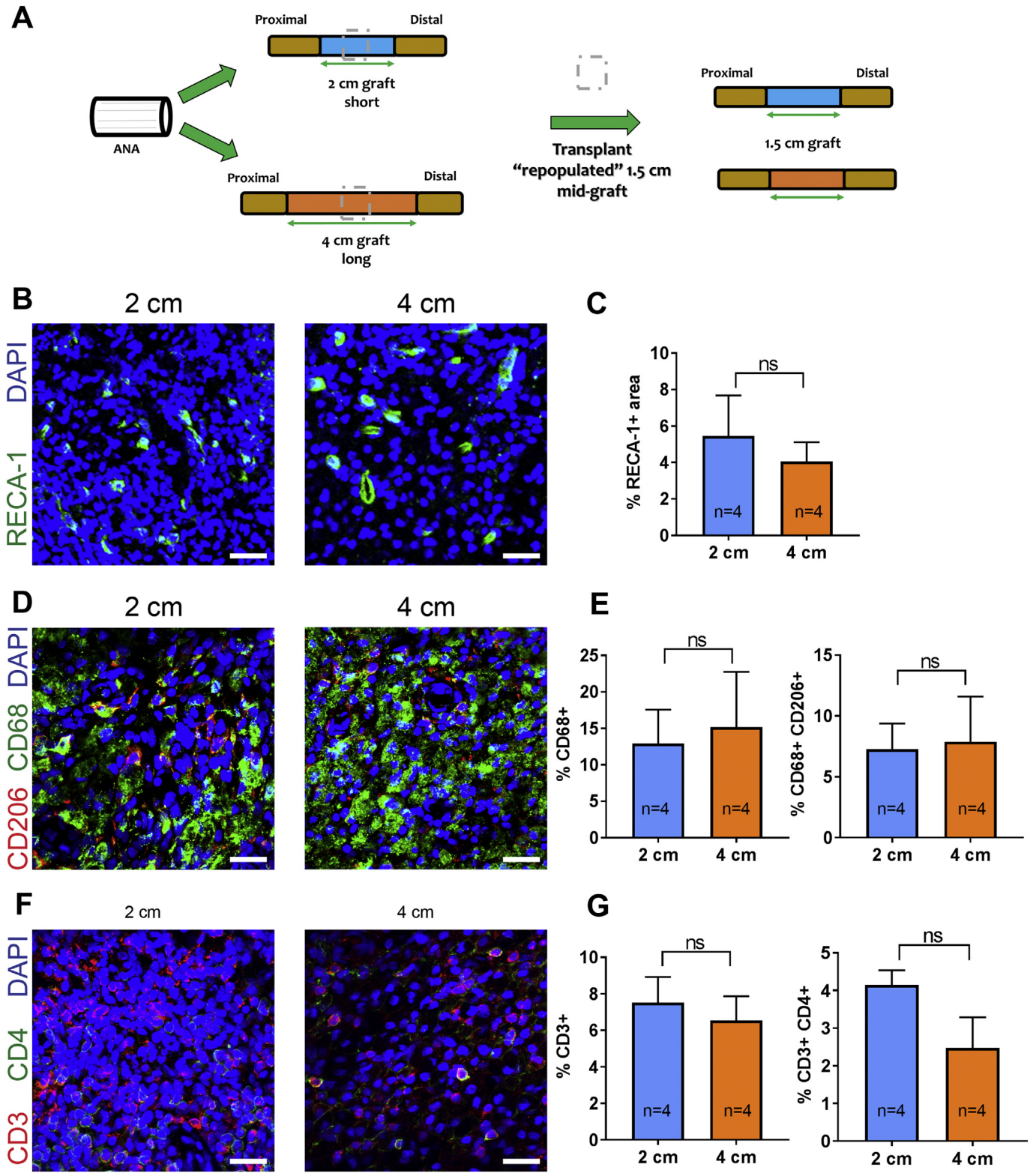

Fig. 7. ANA length functionally limits angiogenesis and T cell accumulation within ANAs. A) Schematic of experimental procedures for "re-grafting" short or long ANAs. Two weeks after re-grafting, mid-graft was assessed using IHC. B) Representative images for RECA-1 (green) and C) quantification of RECA-1+ area. D) Representative images for CD68 (green) and CD206 (red) and E) quantification of the proportion of CD68+ cells and CD68 + CD206+ cells. F) Representative images for CD3 (red) and CD4 (green) and G) quantification of the proportion of CD3+ cells and CD3 + CD4+ cells. Data represented as mean ± SD; ns: not significant. Scale bars represent 40 μm. (For interpretation of the references to colour in this figure legend, the reader is referred to the web version of this article.)

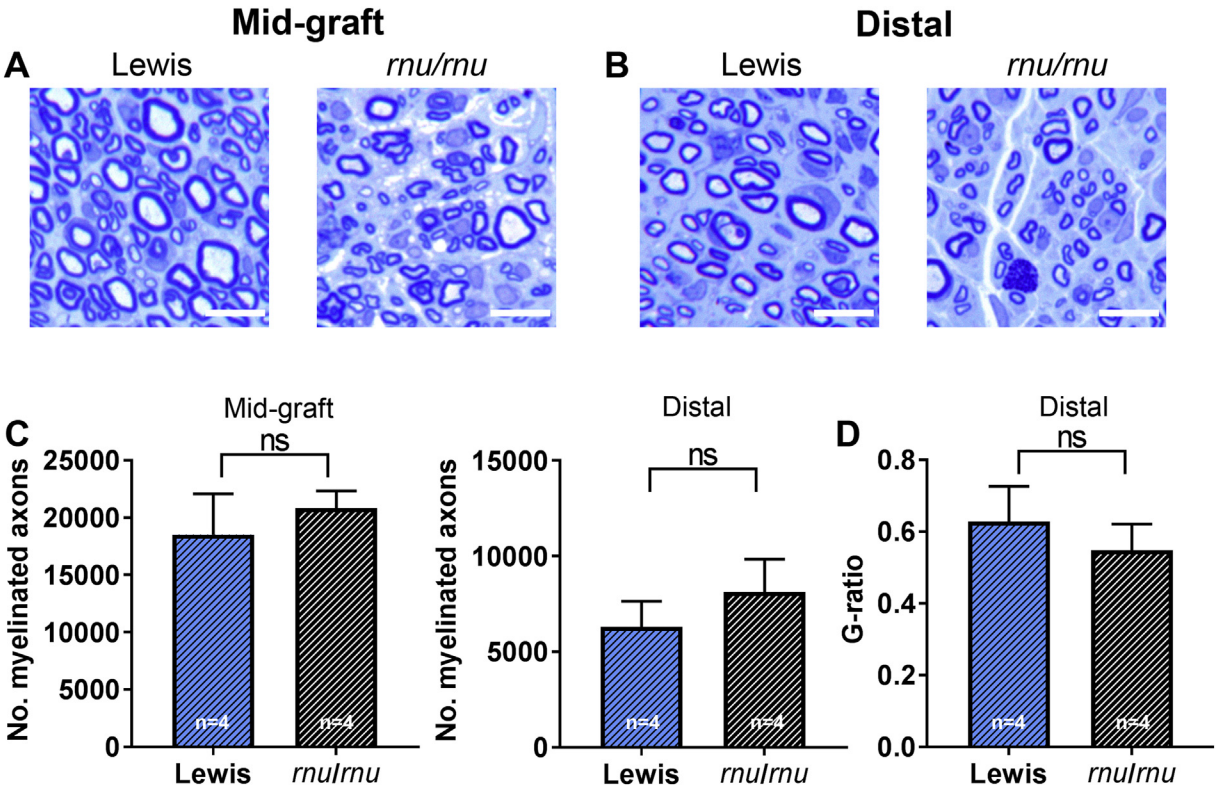

Fig. 8. T cell deficiency does not affect axon regeneration across long (4 cm) isografts. Eight weeks after nerve repair using 4 cm isografts in Lewis or rnu/rnu rats, the extent of nerve regeneration to the mid-graft of ANA and distal nerve was quantified. Representative histological images of nerve at A) mid-graft and B) distal nerve are shown, where white scale bar is 20 μm. C) Quantification of myelinated axons in the mid-graft and distal nerve. D) Quantification of G-ratio in the distal nerve of Lewis or rnu/rnu rats. Data represented as mean ± SD; ns: not significant.

within long ANAs, we assessed if ANA length contributed to this outcome. Two weeks after re-grafting shortened ANAs (Fig. 7A), there was no significant differences in the proportion of RECA-1$^+$ area between re-grafts derived from 2 cm or 4 cm ANAs (Fig. 7B). Similarly, we found that there were no significant differences in the proportion of CD68$^+$ (Fig. 7C) or CD3$^+$ cells (Fig. 7D) among the re-grafted ANAs. This outcome suggests that observed differences in angiogenesis and the immune response between short and long ANAs is due to ANA length.

3.7. T cell deficiency impairs nerve regeneration across ANAs

To assess whether and at what conditions T cells contributed to regeneration, sciatic nerves were repaired in T cell deficient rat models. Eight weeks after nerve repair using isografts, there were no significant differences in the number of regenerated myelinated axons at the mid-graft or distal nerve in athymic (rnu/rnu) rats compared to Lewis rats ($n = 4$ for both groups; Fig. 8A-C). Furthermore, examination of the ratio of axonal myelination revealed Lewis rats had no differences in G-ratio to athymic rats (Fig. 8D). These sets of experiments demonstrate that T cells have limited impact on axonal regeneration when regeneration across the graft does not require substantial cell repopulation of the graft.

To determine if T cells affected regeneration across ANAs, we repaired nerve defects using 2 or 4 cm ANAs. In long (4 cm) ANAs, axon regeneration to even the mid-graft is limited (< 1000 myelinated axons) in Lewis rats. Therefore, while athymic rats contained *no* axons within even the mid-graft, these results in the 4 cm ANA were not statistical due to the large variability in regeneration in the Lewis 4 cm ANA (Fig. S2). Axon regeneration across 2 cm ANAs was robust in Lewis rats, but axon regeneration was decreased by ~2 fold in athymic rats at the mid-graft, and almost 4 fold at the distal nerve (mid-graft $p = 0.0118$, distal $p < 0.0001$; Fig. 9A-C). To also ensure the allogeneic nature of the ANAs was not a factor, we repaired nerve acellular nerve isografts (ANIs), finding no differences in the number of regenerated myelinated axons within mid-graft or across 2 cm ANAs to the distal nerve (Fig. S3).

Furthermore, in rnu/+ heterozygote rats, axon regeneration across 2 cm ANAs was also robust. Compared to rnu/rnu rats, the rnu/+ rats had significantly more myelinated axons in both the mid-graft and distal nerve (mid-graft $p = 0.024$, distal $p = 0.0015$; Fig. 10A-C). As well, we found the myelination degree to be significantly greater (lower G ratio) in the rnu/+ rats than their rnu/rnu counterparts ($p = 0.0088$; Fig. 10D). Comparing relative gastrocnemius muscle mass, recovery was reduced in rnu/rnu rats compared to rnu/+ rats (Fig. 10E). Behavioral assessment using walking track analysis was consistent with the outcome of other regenerative metrics, where rnu/+ rats demonstrated improved SFI scores compared to rnu/rnu rats ($p = 0.013$; Fig. 10F). Overall, these results strongly suggest a causal relationship between T cells and regeneration across ANAs, where T cell deficiency impairs nerve regeneration across ANAs.

4. Discussion

While autografts remain the gold standard for repair of peripheral nerve injuries resulting in a gap between the nerve ends, ANAs have been increasingly used as an alternative to autografts (Isaacs and Browne, 2014; Karabekmez et al., 2009). Yet, despite adequate efficacy for ANAs to repair small gap or small diameter nerve injuries, the capabilities of ANAs to promote regeneration across long nerve gaps has been limited (Zhu et al., 2017). In order to rationally design improvements of alternatives, such as ANAs, there is a need to better understand factors that limit or promote nerve regeneration across ANAs. To that end, we utilized a rat model of sciatic nerve transection with ANA repair to investigate differences in regeneration across short or long

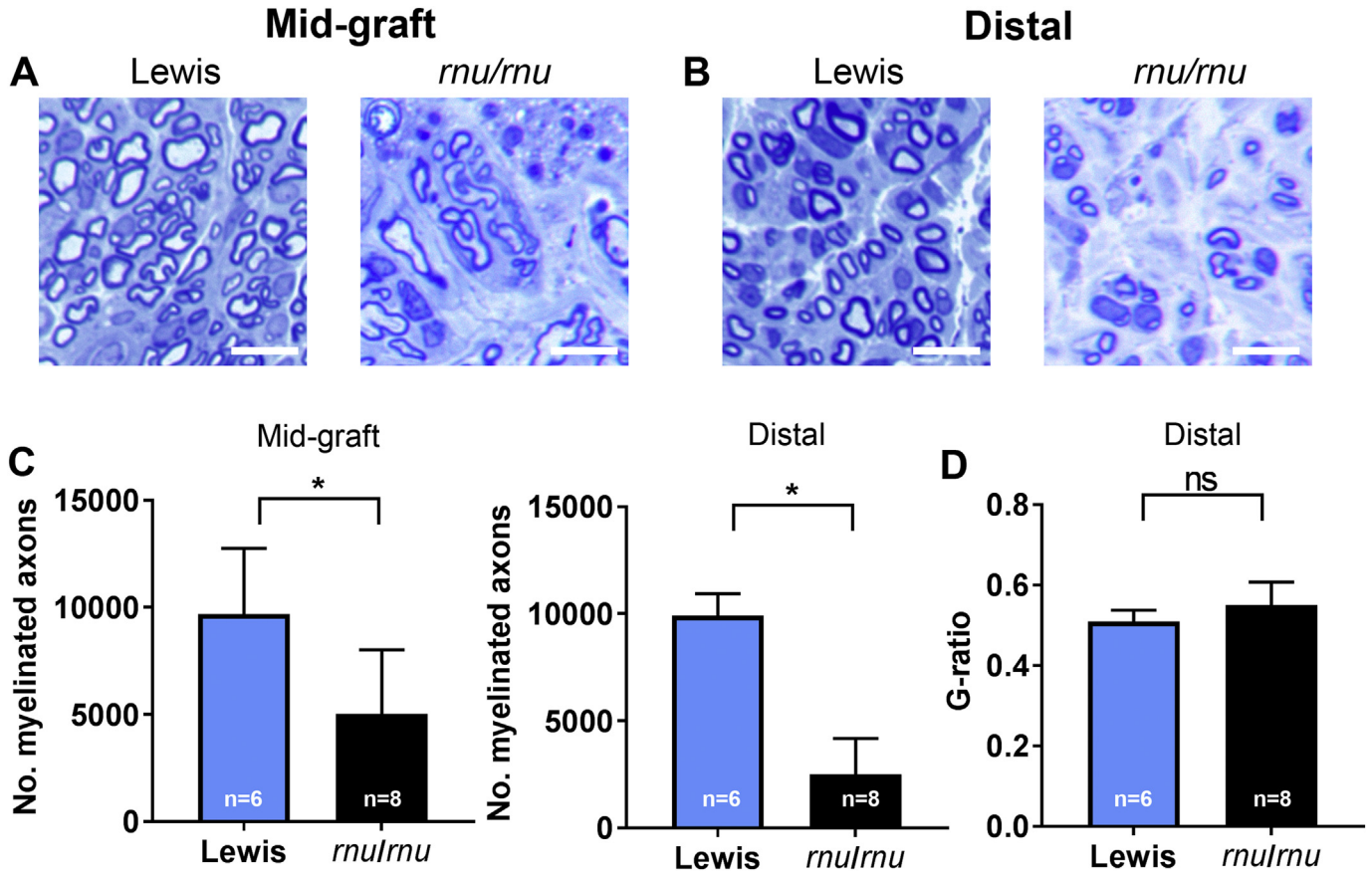

Fig. 9. T cell deficiency affects regeneration across short (2 cm) ANAs. Eight weeks after nerve repair using 2 cm ANAs in Lewis or rnu/rnu rats, the extent of nerve regeneration to the mid-graft of ANA and distal nerve was quantified. Representative histological images of nerve at A) mid-graft and B) distal nerve are shown, where white scale bar is 20 μm. C) Quantification of myelinated axons in the mid-graft and distal nerve. D) Quantification of G-ratio in the distal nerve of Lewis or rnu/rnu rats. Data represented as mean ± SD; * indicates $p < 0.05$. ns: not significant.

ANAs, as short ANAs support regeneration while long ANAs fail to support adequate regeneration. Through these studies, we identified several factors and cell types that could limit nerve regeneration across long ANAs, and provide causal evidence that suggests T cells are critical to promoting nerve regeneration across ANAs.

Previously, we demonstrated that axon regeneration across ANAs is length dependent (Saheb-Al-Zamani et al., 2013), and axon growth arrests prior to reaching even the mid-graft of long ANAs (i.e. > 3 cm) (Poppler et al., 2016). These studies primarily suggested that differences in axon regeneration across longer ANAs was mainly attributable to differences in the ANA environment rather than an innate deficiency of neurons to regenerate their axons across longer nerve grafts (Poppler et al., 2016). Our present studies are consistent with these findings. We saw that the SCs within shorter ANAs, which supported robust axon regeneration, displayed a phenotype distinct from SCs in longer ANAs. Unlike those in the longer ANAs, the SCs in the shorter ANAs are more proliferative and express higher levels of myelination related genes. SCs are known to acquire a “repair” phenotype following nerve injury in which they down regulate myelination genes and upregulate repair related genes, such as growth factors (Arthur-Farraj et al., 2012). Interestingly, in our study, the SCs within longer ANAs expressed lower levels of myelination genes, yet did not express higher level of repair related genes such as *C-Jun*, *Mmp9*, *Gdnf* and *Gap43*. This finding suggests that SCs in longer ANAs may adopt a phenotype that is distinct from either repair or myelination.

To more thoroughly explore why SCs were different between ANAs based on length, we examined key regenerative processes prior to the substantial repopulation of ANAs by SCs. Blood vessels are essential to axonal regeneration and the migration of SCs into sites of injury (Cattin et al., 2015). Given the reduced number of SCs within longer ANAs, it is possible that delayed angiogenesis contributed to reduced SC number and altered phenotype within long ANAs. Previous studies have shown that compared to the gold-standard autografts, acellular scaffolds used to repair nerve have reduced revascularization, suggesting an innately slow process of endothelial cell repopulation of the scaffolds. Thus, longer length ANAs may require a greater amount of time for angiogenesis to complete, leading to delayed or disrupted revascularization. Our data here demonstrated that longer ANAs have disrupted angiogenesis compared to shorter ANAs.

Since macrophages are critical to promoting angiogenesis, we initially hypothesized that reduced angiogenesis was due to either a reduced infiltration of macrophages or an altered phenotype of macrophages in long ANAs. Surprisingly, we did not observe obvious differences in macrophages between 2 cm vs 4 cm ANAs at 2 weeks. In fact, macrophage quantities were not impacted until week 4, even though changes to angiogenesis were evident by week 2. Furthermore, the proportion of macrophages that express CD206, a prominent marker of their anti-inflammatory phenotype, were not different between 2 cm and 4 cm ANA despite higher IL-4 gene expression detected in 2 cm ANAs. This outcome was counterintuitive given the known role of IL-4 promoting a $CD206^+$ macrophage phenotype (Bosurgi et al., 2017). However, the simultaneous elevated expression of IFN-γ in 2 cm ANAs may have prevented alternative activation of macrophages in vivo (Appelberg et al., 1992). Given similar infiltration of macrophages into ANAs of either length early during regeneration (i.e. 2 weeks), the reduced angiogenesis observed in long ANAs is unlikely initially caused by macrophages alone.

The most significant finding of the studies was our observation of

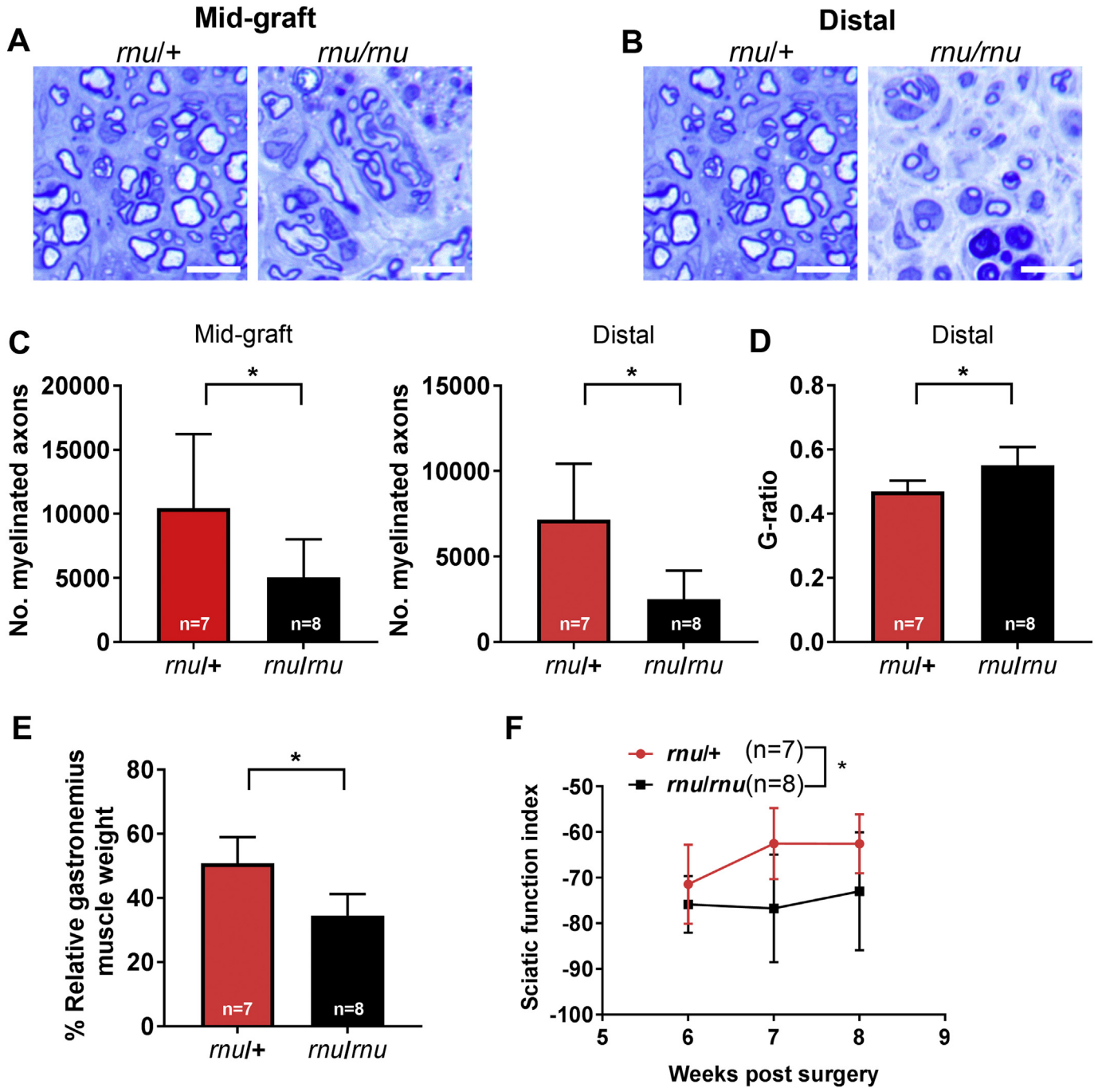

Fig. 10. T cell deficiency affects regeneration across short (2 cm) ANAs. Eight weeks after nerve repair using 2 cm ANAs in rnu/+ or rnu/rnu rats, the extent of nerve regeneration to the mid-graft of ANA and distal nerve was quantified. Representative histological images of nerve at A) mid-graft and B) distal nerve are shown, where white scale bar is 20 μm. C) Quantification of myelinated axons in the mid-graft and distal nerve. D) Quantification of myelination ratio in distal nerve. E) Relative gastrocnemius muscle weight was measured at 8 weeks. F) Sciatic function index was measured from 6 to 8 weeks after repair. Data represented as mean ± SD; * indicates $p < 0.05$.

reduced T cell numbers within long ANAs compared to short ANAs. Concomitant with reduced T cell accumulation at week 2 in 2 cm compared to 4 cm ANAs, we also found significantly reduced cytokine expression with 4 cm ANAs (IFN-γ, IL-2, IL-4, and IL-13). These results suggest that T cells provide or regulate the level of inflammatory cytokines within ANAs. Interestingly, IFN-γ, IL-4, IL-10, and IL-13 have all been shown to be important for regeneration in a variety of organ systems (Cheng et al., 2008; Goh et al., 2013; Horsley et al., 2003; Mokarram et al., 2012). While anti-inflammatory cytokines have been shown to be important for activating gene expression in macrophages to promote tissue regeneration resolution after injury, inflammatory cytokines have been found to promote cell infiltration to sites of injury. Therefore, it is possible that T cells mediate nerve regeneration across ANAs via regulation of inflammatory cytokines. Interestingly, we found that while cells in 2 cm ANAs have greater expression of IL-4 and IFN-γ, T cells did not upregulate their expression of IL-4 compared to splenic T cells. Rather, our data demonstrated that ANA infiltrating T cells, at least early on, upregulate their expression of IFN-γ, a Th1 cytokine that promotes inflammation. While high levels of exogenous IFN-γ have been shown to be detrimental to nerve regeneration, physiological

levels of IFN-γ have been found to be beneficial to regeneration. Furthermore, previous studies have found that low levels of IFN-γ promote SC proliferation. Indeed, when SCs are cultured with IFN-γ at these low levels, the SCs become more proliferative, and express higher levels of GDNF, a growth factor important for nerve regeneration (Fig. S4).

Based on these findings, we directly examined the role of T cells on nerve regeneration across cellular and acellular grafts. When nerve was repaired using an isograft (cellular), the absence of T cells did not significantly deter axonal regeneration. This finding is consistent with previous studies showing that a lack of adaptive immunity did not inhibit regeneration following a nerve crush injury (Bombeiro et al., 2016). Conversely, when nerve was repaired using ANA, axonal regeneration and recovery was significantly diminished when T cells were absent. For nerves repaired with ANAs, the loss of T cells is associated with reduced number of myelinated axons, reduced axonal myelination, and reduced functional recovery. It is unlikely that T cells directly act on neurons to significantly promote their survival and regeneration of axons. If they did, we would have expected reduced axonal regeneration when athymic rats were repaired with isografts. Given that loss of T cells significantly reduced nerve regeneration from ANA repair, it suggests that the neuronal impact of T cells is limited. Rather, the significant differences in nerve regeneration across ANAs in athymic rats compared to their heterozygous counterparts suggest that T cells may play a greater role in the repopulation or regulation of cells within the ANA environment.

In conclusion, our study demonstrated that long compared to short ANAs are repopulated with Schwann cells having an altered phenotype, contain reduced angiogenesis and T cell accumulation, and contain reduced expression of select inflammatory cytokines. T cells likely play a major role in nerve regeneration across ANAs, as a T cell deficiency resulted in reduced regeneration of sciatic nerve through even short ANAs. This finding was unique to ANAs, as regeneration across cellular isografts was unaffected. Our data therefore provides additional mechanistic insight into the cause for failed regeneration in long nerve defects, and may have relevance to regeneration of other tissues where acellular scaffolds are used to promote healing.

Funding

This work was supported in part by the National Institutes of Neurological Disorders and Stroke of the National Institutes of Health (NIH) under award numbers R01 NS086773 and P30 NS057105 to Washington University and by a Pilot Project Award from the Hope Center for Neurological Disorders at Washington University. The content is solely the responsibility of the authors and does not represent the views of the NIH or Washington University.

Appendix A. Supplementary data

Supplementary data to this article can be found online at https://doi.org/10.1016/j.expneurol.2019.05.009.

References

Appelberg, R., Orme, I.M., Pinto de Sousa, M.I., Silva, M.T., 1992. In vitro effects of interleukin-4 on interferon-gamma-induced macrophage activation. Immunology 76, 553–559.

Arthur-Farraj, P.J., Latouche, M., Wilton, D.K., Quintes, S., Chabrol, E., Banerjee, A., Woodhoo, A., Jenkins, B., Rahman, M., Turmaine, M., 2012. C-Jun reprograms Schwann cells of injured nerves to generate a repair cell essential for regeneration. Neuron 75, 633–647.

Bombeiro, A.L., Santini, J.C., Thomé, R., Ferreira, E.R.L., Nunes, S.L.O., Moreira, B.M., Bonet, I.J.M., Sartori, C.R., Verinaud, L., Oliveira, A.L.R., 2016. Enhanced immune response in immunodeficient mice improves peripheral nerve regeneration following axotomy. Front. Cell. Neurosci. 10, 151.

Bosurgi, L., Cao, Y.G., Cabeza-Cabrerizo, M., Tucci, A., Hughes, L.D., Kong, Y., Weinstein, J.S., Licona-Limon, P., Schmid, E.T., Pelorosso, F., Gagliani, N., Craft, J.E., Flavell, R.A., Ghosh, S., Rothlin, C.V., 2017. Macrophage function in tissue repair and remodeling requires IL-4 or IL-13 with apoptotic cells. Science 356, 1072–1076. https://doi.org/10.1126/science.aai8132.

Burzyn, D., Kuswanto, W., Kolodin, D., Shadrach, J.L., Cerletti, M., Jang, Y., Sefik, E., Tan, T.G., Wagers, A.J., Benoist, C., Mathis, D., 2013. A special population of regulatory T cells potentiates muscle repair. Cell 155, 1282–1295. https://doi.org/10.1016/j.cell.2013.10.054.

Cattin, A.-L., Burden, J.J., VanEmmenis, L., Mackenzie, F.E., Hoving, J.J.A., Calavia, N.G., Guo, Y., McLaughlin, M., Rosenberg, L.H., Quereda, V., 2015. Macrophage-induced blood vessels guide Schwann cell-mediated regeneration of peripheral nerves. Cell 162, 1127–1139.

Cattin, A.-L., Lloyd, A.C., 2016. The multicellular complexity of peripheral nerve regeneration. Curr. Opin. Neurobiol. 39, 38–46. https://doi.org/10.1016/j.conb.2016.04.005.

Cheng, M., Nguyen, M.-H., Fantuzzi, G., Koh, T.J., 2008. Endogenous interferon-γ is required for efficient skeletal muscle regeneration. Am. J. Physiol. Physiol. 294, C1183–C1191.

Epelman, S., Liu, P.P., Mann, D.L., 2015. Role of innate and adaptive immune mechanisms in cardiac injury and repair. Nat. Rev. Immunol. 15, 117.

Ghislain, J., Charnay, P., 2006. Control of myelination in Schwann cells: a Krox20 cis-regulatory element integrates Oct6, Brn2 and Sox10 activities. EMBO Rep. 7, 52–58.

Goh, Y.P.S., Henderson, N.C., Heredia, J.E., Eagle, A.R., Odegaard, J.I., Lehwald, N., Nguyen, K.D., Sheppard, D., Mukundan, L., Locksley, R.M., 2013. Eosinophils secrete IL-4 to facilitate liver regeneration. Proc. Natl. Acad. Sci. 110, 9914–9919.

Hesketh, M., Sahin, K.B., West, Z.E., Murray, R.Z., 2017. Macrophage phenotypes regulate scar formation and chronic wound healing. Int. J. Mol. Sci. 18, 1545.

Hoben, G.M., Ee, X., Schellhardt, L., Yan, Y., Hunter, D.A., Moore, A.M., Snyder-Warwick, A.K., Stewart, S., Mackinnon, S.E., Wood, M.D., 2018. Increasing nerve autograft length increases senescence and reduces regeneration. Plast. Reconstr. Surg. 142, 952–961.

Horsley, V., Jansen, K.M., Mills, S.T., Pavlath, G.K., 2003. IL-4 acts as a myoblast recruitment factor during mammalian muscle growth. Cell 113, 483–494.

Hunter, D.A., Moradzadeh, A., Whitlock, E.L., Brenner, M.J., Myckatyn, T.M., Wei, C.H., Tung, T.H.H., Mackinnon, S.E., 2007. Binary imaging analysis for comprehensive quantitative histomorphometry of peripheral nerve. J. Neurosci. Methods 166, 116–124.

Ijkema-Paassen, J., Jansen, K., Gramsbergen, A., Meek, M.F., 2004. Transection of peripheral nerves, bridging strategies and effect evaluation. Biomaterials. https://doi.org/10.1016/S0142-9612(03)00504-0.

Irigoyen, M.P., Caro, M.T., Andrés, E.P., Manrique, A.B., Rey, M.V., Woodhoo, A., 2018. Isolation and purification of primary rodent Schwann cells. In: Myelin. Springer, pp. 81–93.

Isaacs, J., Browne, T., 2014. Overcoming short gaps in peripheral nerve repair: conduits and human acellular nerve allograft. Hand 9, 131–137.

Ishii, H., Jin, X., Ueno, M., Tanabe, S., Kubo, T., Serada, S., Naka, T., Yamashita, T., 2012. Adoptive transfer of Th1-conditioned lymphocytes promotes axonal remodeling and functional recovery after spinal cord injury. Cell Death Dis. 3, e363.

Jaquet, J.B., Luijsterburg, A.J., Kalmijn, S., Kuypers, P.D., Hofman, A., Hovius, S.E., 2001. Median, ulnar, and combined median-ulnar nerve injuries: functional outcome and return to productivity. J. Trauma 51, 687–692. https://doi.org/10.1097/00005373-200110000-00011.

Karabekmez, F.E., Duymaz, A., Moran, S.L., 2009. Early Clinical Outcomes with the Use of Decellularized Nerve Allograft for Repair of Sensory Defects within the Hand.

Kawamura, D.H., Hadlock, T.A., Fox, I.K., Brenner, M.J., Hunter, D.A., Mackinnon, S.E., 2005. Regeneration through nerve isografts is independent of nerve geometry. J. Reconstr. Microsurg. 21, 243–249.

Lavine, K.J., Epelman, S., Uchida, K., Weber, K.J., Nichols, C.G., Schilling, J.D., Ornitz, D.M., Randolph, G.J., Mann, D.L., 2014. Distinct macrophage lineages contribute to disparate patterns of cardiac recovery and remodeling in the neonatal and adult heart. Proc. Natl. Acad. Sci. 111, 16029–16034.

Loots, M.A.M., Lamme, E.N., Zeegelaar, J., Mekkes, J.R., Bos, J.D., Middelkoop, E., 1998. Differences in cellular infiltrate and extracellular matrix of chronic diabetic and venous ulcers versus acute wounds. J. Invest. Dermatol. 111, 850–857.

Lutz, A.B., 2014. Purification of schwann cells from the neonatal and injured adult mouse peripheral nerve. Cold Spring Harb Protoc 2014, 1312.

Mokarram, N., Dymanus, K., Srinivasan, A., Lyon, J.G., Tipton, J., Chu, J., English, A.W., Bellamkonda, R.V., 2017. Immunoengineering nerve repair. Proc. Natl. Acad. Sci. 114, E5077–E5084.

Mokarram, N., Merchant, A., Mukhatyar, V., Patel, G., Bellamkonda, R.V., 2012. Effect of modulating macrophage phenotype on peripheral nerve repair. Biomaterials 33, 8793–8801. https://doi.org/10.1016/j.biomaterials.2012.08.050.

Nishimura, S., Manabe, I., Nagasaki, M., Eto, K., Yamashita, H., Ohsugi, M., Otsu, M., Hara, K., Ueki, K., Sugiura, S., 2009. CD8+ effector T cells contribute to macrophage recruitment and adipose tissue inflammation in obesity. Nat. Med. 15, 914–920.

Poppler, L.H., Ee, X., Schellhardt, L., Hoben, G.M., Pan, D., Hunter, D.A., Yan, Y., Moore, A.M., Snyder-Warwick, A.K., Stewart, S.A., 2016. Axonal growth arrests after an increased accumulation of Schwann cells expressing senescence markers and stromal cells in acellular nerve allografts. Tissue Eng. Part A 22, 949–961.

Pull, S.L., Doherty, J.M., Mills, J.C., Gordon, J.I., Stappenbeck, T.S., 2005. Activated macrophages are an adaptive element of the colonic epithelial progenitor niche necessary for regenerative responses to injury. Proc. Natl. Acad. Sci. 102, 99–104.

Sadtler, K., Estrellas, K., Allen, B.W., Wolf, M.T., Fan, H., Tam, A.J., Patel, C.H., Luber, B.S., Wang, H., Wagner, K.R., 2016. Developing a pro-regenerative biomaterial scaffold microenvironment requires T helper 2 cells. Science 352, 366–370.

Saheb-Al-Zamani, M., Yan, Y., Farber, S.J., Hunter, D.A., Newton, P., Wood, M.D., Stewart, S.A., Johnson, P.J., Mackinnon, S.E., 2013. Limited regeneration in long acellular nerve allografts is associated with increased Schwann cell senescence. Exp. Neurol. 247, 165–177. https://doi.org/10.1016/j.expneurol.2013.04.011.

Sindrilaru, A., Peters, T., Wieschalka, S., Baican, C., Baican, A., Peter, H., Hainzl, A., Schatz, S., Qi, Y., Schlecht, A., 2011. An unrestrained proinflammatory M1 macrophage population induced by iron impairs wound healing in humans and mice. J. Clin. Invest. 121, 985–997.

Stratton, J.A., Holmes, A., Rosin, N.L., Sinha, S., Vohra, M., Burma, N.E., Trang, T., Midha, R., Biernaskie, J., 2018. Macrophages regulate Schwann cell maturation after nerve injury. Cell Rep. 24, 2561–2572.

Taylor, C.A., Braza, D., Rice, J.B., Dillingham, T., 2008. The incidence of peripheral nerve injury in extremity trauma. Am. J. Phys. Med. Rehabil. 87.

Walsh, J.T., Hendrix, S., Boato, F., Smirnov, I., Zheng, J., Lukens, J.R., Gadani, S., Hechler, D., Gölz, G., Rosenberger, K., 2015. MHCII-independent CD4+ T cells protect injured CNS neurons via IL-4. J. Clin. Invest. 125, 699–714.

Whitlock, E.L., Tuffaha, S.H., Luciano, J.P., Yan, Y., Hunter, D.A., Magill, C.K., Moore, A.M., Tong, A.Y., Mackinnon, S.E., Borschel, G.H., 2009. Processed allografts and type I collagen conduits for repair of peripheral nerve gaps. Muscle Nerve 39, 787–799.

Xeroulis, G.J., Park, J., Moulton, C.-A., Reznick, R.K., LeBlanc, V., Dubrowski, A., 2007. Teaching suturing and knot-tying skills to medical students: a randomized controlled study comparing computer-based video instruction and (concurrent and summary) expert feedback. Surgery 141, 442–449.

Yan, Y., Hunter, D.A., Schellhardt, L., Ee, X., Snyder-Warwick, A.K., Moore, A.M., Mackinnon, S.E., Wood, M.D., 2018. Nerve stepping stone has minimal impact in aiding regeneration across long acellular nerve allografts. Muscle Nerve 57, 260–267.

Zhang, J., Xiao, Z., Qu, C., Cui, W., Wang, X., Du, J., 2014. CD8 T cells are involved in skeletal muscle regeneration through facilitating MCP-1 secretion and Gr1high macrophage infiltration. J. Immunol. 1303486.

Zhu, S., Liu, J., Zheng, C., Gu, L., Zhu, Q., Xiang, J., He, B., Zhou, X., Liu, X., 2017. Analysis of human acellular nerve allograft reconstruction of 64 injured nerves in the hand and upper extremity: a 3 year follow-up study. J. Tissue Eng. Regen. Med. 11, 2314–2322.